Acta Mechanica 193, 141–150 (2007)
DOI 10.1007/s00707-006-0434-4
Printed in The Netherlands

Acta Mechanica

Lamb wave excitation with piezoelectric wafers – an analytical approach

S. von Ende, Hamburg, **I. Schäfer**, Kiel, and **R. Lammering**, Hamburg, Germany

Received November 2, 2006
Published online: February 14, 2007

Summary. The excitation of Lamb waves with piezoelectric wafers is analytically modeled with help of the Fourier transform method combined with the Residue theorem for the inverse transform. The calculation utilizes a decomposition of the load in a symmetric and an antisymmetric part and leads to the well known Rayleigh-Lamb-frequency equation. A solution for the whole waveguide continuum including the excitation zone is given. It is shown that the solution satisfies not only the underlying partial differential equations but also the given boundary conditions which has not been verified before.

1 Introduction

The fast and efficient detection of hidden structural damages of plates and shells is the main goal of structural health monitoring (SHM) systems. SHM allows to adjust maintenance intervals in accordance to the real requirements so that a reduction of the operating costs is expected. From an economical point of view, aerospace structures are of special interest for improved inspection techniques, since a considerable amount of life cycle costs is due to inspection and repair and since damage can lead to catastrophic failure. Moreover, the increasing application of fiber reinforced plastics in lightweight aerospace structures is currently demanding for advanced monitoring systems.

Actually, various SHM systems are under development. Passive systems monitor plates and shells for acoustic emissions which are generated from impacts or newly developing or propagating cracks. In contrast, active systems interact with the structure and analyze the reactions. Examples of active systems are the conventional ultrasonic testing methods and, more recently under development, testing procedures based on Lamb waves. The latter technology benefits from the fact that Lamb waves spread out over large areas of the plate and shell structures under investigation so that they do not need to be scanned.

The main research fields in Lamb wave testing are the correct interpretation of the sensed signals and the development of small, lightweight and low cost transducers for Lamb wave generation and sensing. A multitude of Lamb wave transducers exists, e.g., wedge-, interdigital-, electromagnetic-, capacitive micro machined ultrasonic (CMU) transducers and piezoelectric wafers. In order to develop and optimize these transducers, a fundamental knowledge of the mechanical problem related with Lamb wave generation is necessary. This work aims to contribute to this field of research.

After the description of free, time harmonic plane strain waves in an elastic layer by Lamb [1], Victorov [2] investigated Lamb waves with help of the Fourier transform. More recent work using this method was presented by other authors, cf. [3]–[6]. Alternative approaches have been developed in parallel. In [7] and [8], the resulting fields in the waveguide were expressed by the mode expansion technique which makes use of the eigenmodes of free Lamb waves. Achenbach and Xu [9] described the generation of waves in elastic layers by time harmonic point loads using a membrane carrier wave. To the knowledge of the authors, this publication is the only one with a solution for the resulting fields which is valid throughout the entire waveguide continuum. Further work has been done by Badi et al. [10] who used an equivalent circuit model for describing a CMU-transducer and by Wilcox et al. [11] who defined the excitability of guided waves.

In this work an analytical model for the excitation of Lamb waves with piezoelectric wafers (PW) will be presented. The mechanical system consists of one piezoelectric wafer which is bonded to the upper surface of a plate. In case of wave generation, shear stresses are transfered from the wafer to the plate structure. The mathematical approach for the problem solution makes use of the common Fourier transform and is combined with the Residue theorem. Starting point is a recent paper of Giurgiutiu [6].

The organization of the manuscript is as follows. In the first Section, the governing equations and boundary conditions of the underlying problem are derived. Then, a solution in the wave number domain is specified. After that the application of the Residue theorem for inverse transform is sketched. In the last Section the whole solution procedure is exemplarily shown for the above-mentioned loading case, and it will be verified that the solution satisfies the given boundary conditions. This is only possible because a closed form solution for the entire continuum of the waveguide, containing the excitation zone, has been derived.

2 Description in the time domain

2.1 Lamé-Navier differential equations for elastic infinite plates

The governing differential equations are derived from Newton's second law, using Hooke's law for homogeneous isotropic elastic materials and assuming small strains:

$$(\lambda+\mu)\partial_{ij}\{\mathbf{u}_j[x,y,z,t]\}+\mu\partial_{ll}\{\mathbf{u}_i[x,y,z,t]\}+\rho\mathbf{f}_i[x,y,z,t]=\rho\ddot{\mathbf{u}}_i[x,y,z,t], \tag{1}$$

where $\mathbf{u}_i$ is the displacement field, λ and μ are the Lamé constants, ρ and $\mathbf{f}_i$ are density and body force. Equations (1) are known as the Lamé-Navier differential equations. The partial derivative is written here using the following definition:

$$\partial_{a1\ldots an}\{.\}:=\frac{\partial^n}{\partial_{a1}\ldots\partial_{an}}\{.\}. \tag{2}$$

For the sake of brevity the dependence of the variables is dropped in the following expressions, if they do not change or are not important for understanding.

The displacement field $\mathbf{u}_i$ can be separated in a curl free scalar field φ and a divergence free vector field $\mathbf{\Psi}_i$ with the help of Helmholtz's theorem

$$\mathbf{u}_i=\partial_i\{\varphi\}+\boldsymbol{\epsilon}_{igh}\partial_g\{\mathbf{\Psi}_h\}, \tag{3}$$

where $\boldsymbol{\epsilon}_{igh}$ is the permutation tensor.

With this separation the Lamé-Navier differential equations can be split into two sets of potential equations standing for longitudinal and transversal waves in solids. Following Lamb

[1] we assume a plain strain state and a time harmonic solution $\mathbf{u}_i[x,y]\mathbf{e}^{-\mathbf{i}\omega t}$ for the analysis of plates in the x-y-plane. Therefore Eq. (3) takes the form:

$$\begin{aligned}\mathbf{u}_x[x,y] &= \partial_x\{\varphi[x,y]\} + \partial_y\{\boldsymbol{\Psi}_z[x,y]\},\\ \mathbf{u}_y[x,y] &= \partial_y\{\varphi[x,y]\} - \partial_x\{\boldsymbol{\Psi}_z[x,y]\},\\ \mathbf{u}_z[x,y] &= 0.\end{aligned} \tag{4}$$

Neglecting furthermore the effect of body forces we get the following set of potential equations for waves in infinite elastic plates:

$$\begin{aligned}&\partial_{xx}\{\varphi\} + \partial_{yy}\{\varphi\} + \omega^2\frac{\rho}{2\mu+\lambda}\varphi = 0,\\ &\partial_{xx}\{\boldsymbol{\Psi}_z\} + \partial_{yy}\{\boldsymbol{\Psi}_z\} + \omega^2\frac{\rho}{\mu}\boldsymbol{\Psi}_z = 0.\end{aligned} \tag{5}$$

2.2 Piezoelectric actuator

Lamb waves can be generated by piezoelectric wafers, which are bonded to the surface of the plate. If a voltage is applied to the PW, it is contracting or expanding and is therefore generating a shear stress at the interface between actuator and plate [6]. This is illustrated in Fig. 1.

The stress tensor can be expressed as

$$\mathbf{T}_{ij} = \mu(\partial_j\{\mathbf{u}_i\} + \partial_i\{\mathbf{u}_j\}) + \lambda\partial_l\{\mathbf{u}_l\}\boldsymbol{\delta}_{ij}, \tag{6}$$

where $\boldsymbol{\delta}_{ij}$ is the Kronecker-tensor.

Setting $\mathbf{T}_{yy}[x, y=d] = 0$ and $\mathbf{T}_{yx}[x, y=d] = \tau[x]$ we get the following boundary conditions:

$$\begin{aligned}&(\lambda+2\mu)\partial_{yy}\{\varphi[x,y=d]\} - 2\mu\partial_{xy}\{\boldsymbol{\Psi}_z[x,y=d]\} + \lambda\partial_{xx}\{\varphi[x,y=d]\} = 0,\\ &\mu(\partial_{yy}\{\boldsymbol{\Psi}_z[x,y=d]\} + 2\partial_{xy}\{\varphi[x,y=d]\} - \partial_{xx}\{\boldsymbol{\Psi}_z[x,y=d]\}) = \tau[x].\end{aligned} \tag{7}$$

The potential differential equations (5) and boundary conditions (7) describe the entire problem.

3 Solution in the wave number domain - Fourier transform

A common method for solving such surface load problems is to apply the Fourier transform $\tilde{f}(k) = \int_{-\infty}^{\infty} f(x)\mathbf{e}^{-\mathbf{i}kx}dx$ [2], [12].

After obtaining the transform from (5), we get now a set of ordinary differential equations of second order in y for every held wavenumber k:

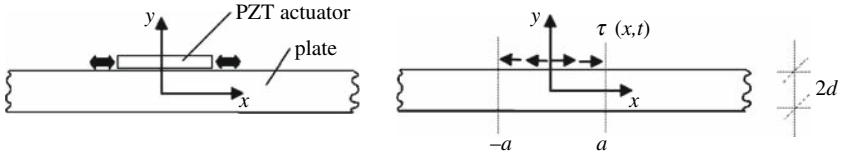

Fig. 1. Modeling of a piezoelectric wafer actuator bonded to a steel plate (left) with a stress boundary condition (right)

$$\begin{aligned}&\partial_{yy}\{\tilde{\varphi}[k,y]\}+p^2\tilde{\varphi}[k,y]=0,\\&\partial_{yy}\{\tilde{\mathbf{\Psi}}_z[k,y]\}+q^2\tilde{\mathbf{\Psi}}_z[k,y]=0,\end{aligned}\tag{8}$$

where $p=\sqrt{kl^2-k^2}$, $q=\sqrt{kt^2-k^2}$, $kl^2=\omega^2\frac{\rho}{2\mu+\lambda}$ and $kt^2=\omega^2\frac{\rho}{\mu}$.

Equations (8) have the general solution

$$\begin{aligned}&\tilde{\varphi}=A_1\sin[py]+A_2\cos[py],\\&\tilde{\mathbf{\Psi}}_z=B_1\sin[qy]+B_2\cos[qy].\end{aligned}\tag{9}$$

Those parts of Eqs. (9) containing the free constants A_2 and B_1 describe symmetric solutions, and terms including A_1 and B_2 contribute to antisymmetric solutions with respect to the plate mid surface. In order to evaluate the unknown constants A_1, A_2, B_1, and B_2 the transformed stress condition at the boundary is used:

$$\begin{aligned}&(\lambda+2\mu)\partial_{yy}\{\tilde{\varphi}[k,y=d]\}-2\mathbf{i}k\mu\partial_y\{\tilde{\mathbf{\Psi}}_z[k,y=d]\}-k^2\lambda\tilde{\varphi}[k,y=d]=0,\\&\mu(\partial_{yy}\{\tilde{\mathbf{\Psi}}_z[k,y=d]\}+2\mathbf{i}k\partial_y\{\tilde{\varphi}[k,y=d]\}+k^2\tilde{\mathbf{\Psi}}_z[k,y=d])=\tilde{\tau}[k].\end{aligned}\tag{10}$$

The symmetric (superscript S) and antisymmetric (superscript A) cases are now considered separately. Then, Eqs. (10) yield an inhomogeneous linear system of equations, from which the unknown constants are evaluated. The decomposition of the load is shown in Fig. 2. The complete solution of the transformed problem can be written as:

$$\tilde{\mathbf{u}}_x[k,y]=\frac{N_x^A[k,y]}{D^A[k]}\tilde{\tau}^A[k]+\frac{N_x^S[k,y]}{D^S[k]}\tilde{\tau}^S[k]\tag{11}$$

and

$$\tilde{\mathbf{u}}_y[k,y]=\frac{N_y^A[k,y]}{D^A[k]}\tilde{\tau}^A[k]+\frac{N_y^S[k,y]}{D^S[k]}\tilde{\tau}^S[k],\tag{12}$$

by which the subsequent quantities are introduced:

$$N_x^A[k,y]=\ q(-(k^2-q^2)\sin[dp]\sin[qy]+2k^2\sin[dq]\sin[py]),\tag{13}$$

$$N_x^S[k,y]=\ q((k^2-q^2)\cos[dp]\cos[qy]-2k^2\cos[dq]\cos[py]),\tag{14}$$

$$N_y^A[k,y]=\ -ik(2pq\cos[py]\sin[dq]+(k^2-q^2)\cos[qy]\sin[dp]),\tag{15}$$

$$N_y^S[k,y]=\ -ik(2pq\cos[dq]\sin[py]+(k^2-q^2)\cos[dp]\sin[qy]),\tag{16}$$

$$D^A[k]=\ \mu(4k^2pq\cos[dp]\sin[dq]+(k^2-q^2)^2\cos[dq]\sin[dp]),\tag{17}$$

$$D^S[k]=\ \mu(4k^2pq\cos[dq]\sin[dp]+(k^2-q^2)^2\cos[dp]\sin[dq]).\tag{18}$$

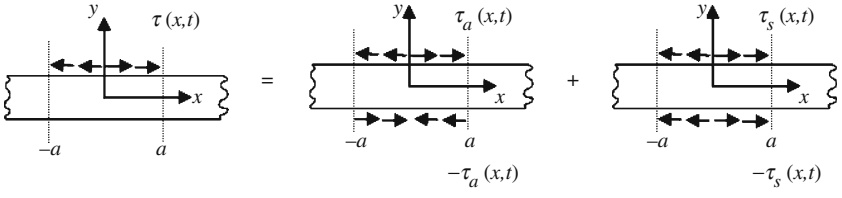

Fig. 2. Decomposition of the boundary condition into symmetric and antisymmetric parts

4 Solution in the time domain – inverse Fourier transform

4.1 Residue theorem

In order to obtain the solution in the time domain one has to calculate the inverse Fourier transform: $f[x] = \frac{1}{2\pi}\int_{-\infty}^{\infty}\tilde{f}[k]\mathbf{e}^{\mathbf{i}kx}dk$. This is the most difficult part of the solution process, and in most cases the direct integration does not work. A common method is to use the Residue theorem, see for example [2], [12] and recently [6]. According to this theorem the integral over a closed path in the complex plane is equal to $2\pi\mathbf{i}$ times the sum of the residues of the enclosed poles. If some poles lie on the path of integration only the half is added. One obtains

$$\begin{aligned}\oint_{\Gamma} F[k]d\Gamma &= \int_{\Gamma_1} F[k]d\Gamma_1 + \int_{-\infty}^{\infty} F[k]dk \\ &= 2\pi\mathbf{i}\sum_{i=1}^{n} Res[F[k], k = k0c_i] + \pi\mathbf{i}\sum_{l=1}^{m} Res[F[k], k = k0r_l],\end{aligned} \tag{19}$$

where $F[k]$ is a complex function with complex poles at $k0c$ and real poles $k0r$. The path of integration has to be chosen properly, so that all integrals $\int_{\Gamma_1} F[k]d\Gamma_1$ with exception of the path integral along the real axis evaluate to zero. Then $\int_{-\infty}^{\infty} F[k]dk$ can be replaced by a sum of residues.

In the next two Subsections the integral along path Γ_1 is investigated in detail.

4.2 Branch cut

The integrand of Eq. (19) contains root functions, namely the values p and q in Eqs. (11) and (12), which have been introduced in (8). In this case we additionally have to investigate branch cuts, for details see [13]. Graff [12] states that the evaluation of the integrals along the branch cuts is most formidable. For a similar problem Victorov [2] gives a solution for the displacement field at the surface of the plate outside of the excitation zone.

In our investigations we will show in the following that the additional integrals along the branch cuts evaluate to zero. First we determine the locations of the branch cuts. For the root function $p = \sqrt{kl^2 - k^2}$ it lies on $\{k|kl \le |k|\}$ and for $q = \sqrt{kt^2 - k^2}$ on $\{k|kt \le |k|\}$. Now we are able to select the path of integration, see Fig. 3. The path in the upper half plane along the branch cut can be parameterized using $k = r_u\mathbf{e}^{\mathbf{i}\pi} = -r_u$ with $r_u > 0$ and in the lower half plane $k = r_l\mathbf{e}^{-\mathbf{i}\pi} = -r_l$ with $r_l > 0$. Because there are two branch cuts at the negative axis, the path of integration has to be divided. We get the following additional integrals:

$$\begin{aligned}I_{u1} &= \int_{r_u=\infty}^{kt} \tilde{\mathbf{u}}_x[-r_u, y]\mathbf{e}^{\mathbf{i}(-r_u)x}(-dr_u), \\ I_{u2} &= \int_{r_u=kt}^{kl} \tilde{\mathbf{u}}_x[-r_u, y]\mathbf{e}^{\mathbf{i}(-r_u)x}(-dr_u), \\ I_{l1} &= \int_{r_l=kl}^{kt} \tilde{\mathbf{u}}_x[-r_l, y]\mathbf{e}^{\mathbf{i}(-r_l)x}(-dr_l), \\ I_{l2} &= \int_{r_l=kt}^{\infty} \tilde{\mathbf{u}}_x[-r_l, y]\mathbf{e}^{\mathbf{i}(-r_l)x}(-dr_l).\end{aligned} \tag{20}$$

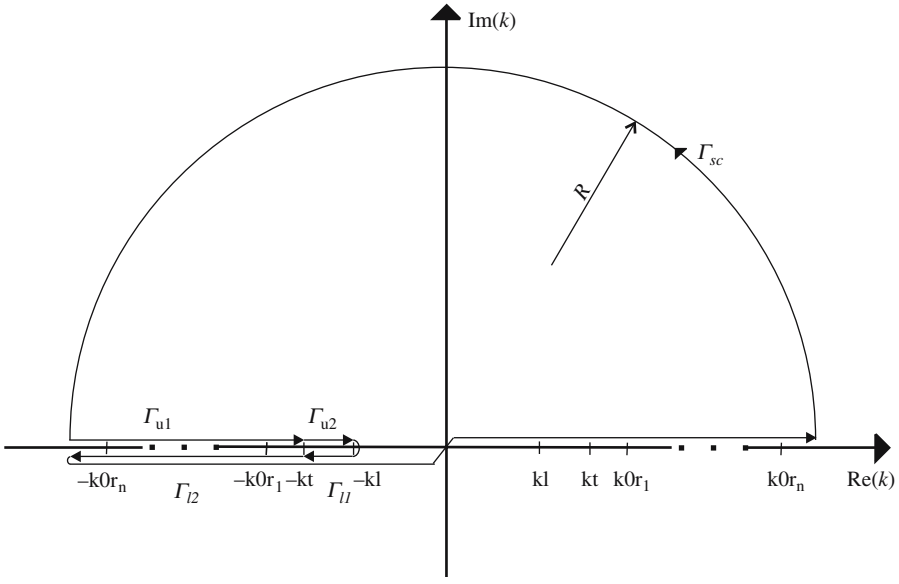

Fig. 3. Sketch of the selected path of integration

In the case under consideration adding up I_{u1} and I_{l2} yields zero and I_{u2} plus I_{l1} is zero, too. This is not a matter of course and holds only because of the special structure of the functions given in Eqs. (11)–(18), which is the result of the underlying mechanical problem.

4.3 Integration of the semi-circle

An investigation of the behavior of the semi circle integral is necessary, because it is not evident that this integration gives zero, if the radius tends to infinity. The given boundary condition $\tilde{\tau}[k]$ has crucial influence.

Even with the simplest integrand one has to make case distinctions. This will be shown by the subsequent example. Consider an integral $f[x] = \frac{1}{2\pi}\int_{-\infty}^{\infty} \mathbf{e}^{\mathbf{i}kx} dk$. There are no residues in $k \in C$. The semi circle is parameterized with $k = R\mathbf{e}^{\mathbf{i}\varphi}$ where $R \to \infty$ and $\varphi \in [0, \pi]$, therefore dk can be replaced by $\mathbf{i}R\mathbf{e}^{\mathbf{i}\varphi}dr$. For $x > 0$ the integral tends to zero if $R \to \infty$. If we solve for $x < 0$ we only get zero, if we integrate along a semi circle in the lower half space: $k = R\mathbf{e}^{-\mathbf{i}\varphi}$. For $x = 0$ the integral does not vanish, it tends to $-\infty$ if $R \to \infty$. Because of Eq. (19) we get the solution $f[x] = \delta[x]$, which is the Dirac distribution. Summarizing we state that at least three case distinctions have to be investigated: (i) $x > 0$, (ii) $x < 0$ and (iii) $x = 0$.

In the next Section the whole solution process is demonstrated for a given stress distribution $\tau[x]$.

5 An example

We investigate an applied shear stress in the form

$$\tau[x] = \tau_0(2H[x] - H[x + a] - H[x - a]), \tag{21}$$

where $H[x]$ is the Heaviside step function, see Fig. 6. The Fourier transform gives

$$\tilde{\tau}[k] = \frac{-\mathbf{i}4\tau_0 \sin^2[\frac{a}{2}k]}{k}. \tag{22}$$

After the integration along the branch cuts evaluate to zero, we have to survey in which cases the integrals of Eqs. (11) and (12) along the semi-circle vanish. Therefore Eq. (22) has to be converted to

$$\tilde{\tau}[k] = \frac{\mathbf{i}\tau_0}{k}(\mathbf{e}^{\mathbf{i}ak} - 2 + \mathbf{e}^{-\mathbf{i}ak}). \tag{23}$$

Now we are able to split the integral (19) into three parts with identical limits, using Eqs. (11)–(12) and (23):

$$\begin{aligned}
\oint_\Gamma F[k]d\Gamma &= \oint_\Gamma \frac{1}{2\pi}\left(\frac{N_x^A[k,y]}{D^A[k]} + \frac{N_x^S[k,y]}{D^S[k]}\right)\frac{1}{2}\tilde{\tau}[k]\mathbf{e}^{\mathbf{i}kx}d\Gamma \\
&= \oint_\Gamma \frac{1}{2\pi}\left(\frac{N_x^A[k,y]}{D^A[k]} + \frac{N_x^S[k,y]}{D^S[k]}\right)\frac{\mathbf{i}\tau_0}{2k}\mathbf{e}^{\mathbf{i}k(x+a)}d\Gamma \\
&\quad + \oint_\Gamma \frac{1}{2\pi}\left(\frac{N_x^A[k,y]}{D^A[k]} + \frac{N_x^S[k,y]}{D^S[k]}\right)\left(-\frac{\mathbf{i}\tau_0}{k}\right)\mathbf{e}^{\mathbf{i}kx}d\Gamma \\
&\quad + \oint_\Gamma \frac{1}{2\pi}\left(\frac{N_x^A[k,y]}{D^A[k]} + \frac{N_x^S[k,y]}{D^S[k]}\right)\frac{\mathbf{i}\tau_0}{2k}\mathbf{e}^{\mathbf{i}k(x-a)}d\Gamma,
\end{aligned} \tag{24}$$

where $\tilde{\tau}^A[k] = \tilde{\tau}^S[k] = \frac{1}{2}\tilde{\tau}[k]$. This is exemplarily done for $\mathbf{u}_x$ and has to be repeated for $\mathbf{u}_y$.

We make different case distinctions for each integral in Eq. (24). It is evident that these are (i) $x > -a$, (ii) $x = -a$ and (iii) $x < -a$, e.g. for the first integral.

Subsequently we will give the explicit inverse transform only for the first case of the first integral, all other cases work the same way. The path integral along the semi-circle in the upper half plane evaluates to zero, thus we can write using the expression $Res[N[k]/D[k], k = k_n] = N[k_n]/D'[k_n]$ for the residue of a fraction at the simple pole k_n:

$$\begin{aligned}
\mathbf{u}_x^{11}[x,y] &= \int_{-\infty}^{\infty} \frac{1}{2\pi}\left(\frac{N_x^A[k,y]}{D^A[k]} + \frac{N_x^S[k,y]}{D^S[k]}\right)\frac{\mathbf{i}\tau_0}{2k}\mathbf{e}^{\mathbf{i}k(x+a)}dk \\
&= -\frac{\tau_0}{4}\left(\sum_{j=1}^{m}\frac{N_x^A[k=\xi_j,y]}{\partial_k\{D^{Ah}[k=\xi_j]\}}\mathbf{e}^{\mathbf{i}\xi_j(x+a)}\right. \\
&\quad \left. + \sum_{l=1}^{n}\frac{N_x^S[k=\zeta_l,y]}{\partial_k\{D^{Sh}[k=\zeta_l]\}}\mathbf{e}^{\mathbf{i}\zeta_l(x+a)}\right),
\end{aligned} \tag{25}$$

where $D^{Ah}[k] = D^A[k]k$ and $D^{Sh}[k] = D^S[k]k$. The values ξ and ζ are simple poles of the fractions $\frac{N_x^A[k,y]}{D^{Ah}[k]}$ and $\frac{N_x^S[k,y]}{D^{Sh}[k]}$, respectively. Among others these sets of poles contain all zeros from $D^A[k]$ and $D^S[k]$, which are the already known eigenvalues of the Rayleigh-Lamb-frequency equation for the free Lamb wave. If we sum up over all zeros (negative and positive) we get standing waves, summation over positive values (including zero) gives waves, which are travelling away from the source.

Since these poles are independent from y, we do not only get the inverse transformed results at the surface of the plate but also the complete vector field $\mathbf{u}_i[x,y]$, which is calculated from

$$\mathbf{u}_i = \sum_{n=1}^{3} (\mathbf{u}_i^{n1} + \mathbf{u}_i^{n2} + \mathbf{u}_i^{n3}). \tag{26}$$

In Eq. (26) the term $\mathbf{u}_i^{n2}$ denotes the second case for the $\boldsymbol{n}$-th integral that is needed for evaluating the displacement $\mathbf{u}_i$.

All following results are calculated for a steel plate with the parameters $d = 2.4\,\text{mm}$, $a = 4.5\,\text{mm}$, $Y = 210\,\text{GPa}$, $\nu = 0.3$, $\rho = 7800\,\frac{\text{kg}}{m^3}$, $\tau_0 = 100\,\text{kPa}$ and $\omega = 12000\pi\,\text{Hz}$. At the given frequency, only two propagating modes exist, namely the symmetric S_0 mode and the antisymmetric A_0 mode. In Fig. 4 the displacements along the surface are plotted. Another interesting plot is given in Fig. 5, where the displacements of the asymmetric mode along the thickness of the plate (x-coordinate fixed) are given. It can be seen that $\mathbf{u}_y^A[x, y = d] = \mathbf{u}_y^A[x, y = -d]$ and $\mathbf{u}_x^A[x, y = d] = -\mathbf{u}_x^A[x, y = -d]$ is valid. Since we have computed the complete displacement vector field, it is possible to validate the given boundary condition, using Eq. (6). A plot of $\tau[x]$ and the calculated stress $\mathbf{T}_{yx}[x, y = d]$ is shown in Fig. 6.

6 Conclusions

A closed solution for excited Lamb waves in homogeneous isotropic elastic plates due to time harmonic loading through piezoelectric wafers was presented. This solution is valid for the whole continuum and satisfies the underlying differential equations and boundary conditions. As in the solution given by Achenbach and Xu [9], it is necessary to compute the eigenvalues of the Rayleigh-Lamb-frequency equation. Since this is not possible in a closed form, numerical algorithms of the program Mathematica have been applied.

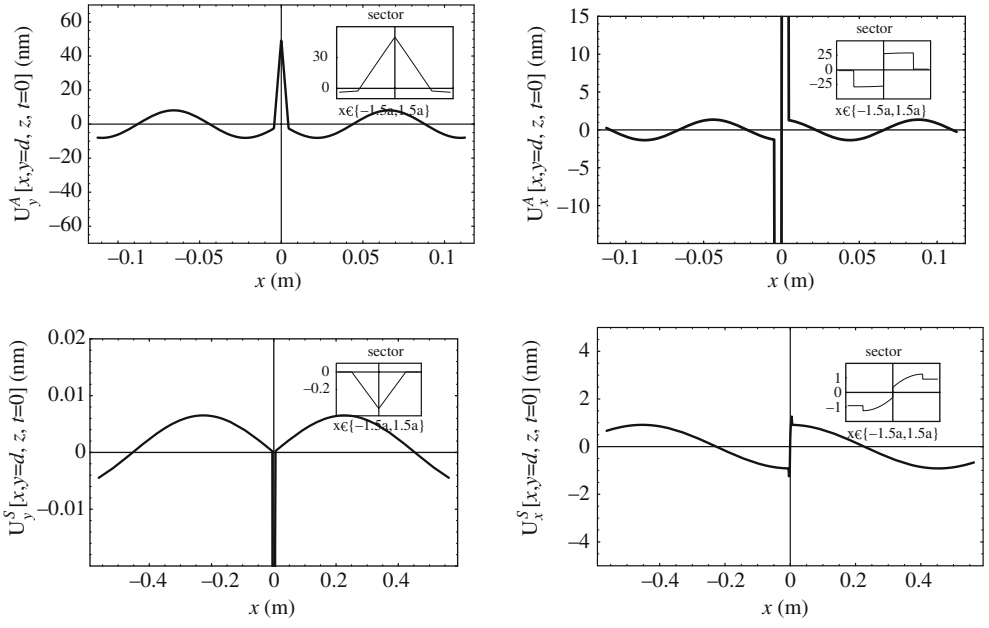

Fig. 4. Plot of the displacement in y- and x-direction of the antisymmetric (top) and symmetric (bottom) Lamb wave at the plate upper surface

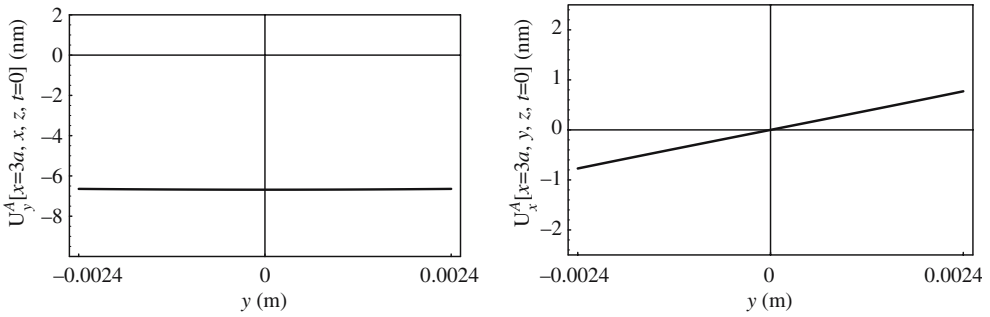

Fig. 5. Plot of the displacement in y- and x-direction of the antisymmetric Lamb wave along the thickness of the plate at a fixed x-coordinate

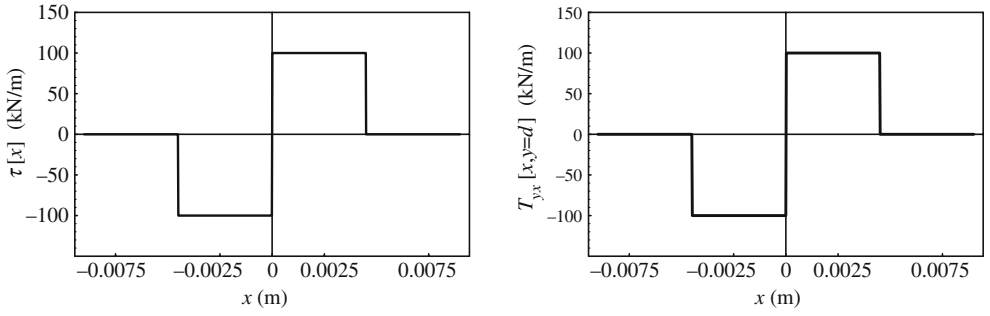

Fig. 6. Comparison of the given boundary condition (left) and the calculated stress T_{yx} at the plate upper surface (right)

References

[1] Lamb, H.: On waves in an elastic plate. Proc. Roy. Soc. Ser. A **93**, 114–128 (1917).
[2] Viktorov, I. A.: Rayleigh and Lamb waves: physical theory and applications. New York: Plenum Press 1967.
[3] Gomilko, A. M., Gorodetskaya, N. S., Meleshko, V. V.: Longitudinal Lamb waves in a semi-infinite elastic layer. Int. Appl. Mech. **27**, 577–581 (1991).
[4] Veidt, M., Liu, T., Kitipornchai, S.: Modelling of Lamb waves in composite laminated plates excited by interdigital transducers. NDT & E International **35**, 437–447 (2002).
[5] Raghavan, A., Cesnik, C. E. S.: Modeling of piezoelectric-based lamb-wave generation and sensing for structural health monitoring. Proc. of SPIE – Smart Structures and Materials **5391**, 419–430 (2004).
[6] Giurgiutiu, V.: Tuned Lamb wave excitation and detection with piezoelectric wafer active sensors for structural health monitoring. J. Intell. Mater. Systems Struct. **16**, 291–305 (2005).
[7] Jia, X.: Modal analysis of Lamb wave generation in elastic plates by liquid wedge transducers. J. Accoust. Soc. Amer. **101**, 834–842 (1997).
[8] Jin, J., Quek, S. T., Wang, Q.: Analytical solution of excitation of Lamb waves in plates by inter-digital transducers. Proc. R. Soc. Lond. A **459**, 1117–1134 (2003).
[9] Achenbach, J. D., Xu, Y.: Wave motion in an isotropic elastic layer generated by a time-harmonic point load of arbitrary direction. J. Acoust. Soc. Amer. **106**, 83–90 (1999).
[10] Badi, M. H., Yaralioglu, G. G., Ergun, A. S., Hansen, S. T., Wong, E. J., Khuri-Yakub, B. T.: Capacitive mircromachined ultrasonic Lamb wave transducers using rectangular membranes. IEEE Transactions on ultrasonics, piezoelectrics and frequenquency control **50**, 1191–1203 (2003).
[11] Wilcox, P. D., Lowe, M. J. S., Cawley, P.: The excitation and detection of Lamb waves with planar coil electromagnetic acoustic transducers. IEEE Transactions on ultrasonics, piezoelectrics and frequenquency control **52**, 2370–2383 (2005).

[12] Graff, K. F.: Wave motion in elastic solids. New York: Dover Publications 1991.
[13] Marsden, J. E., Hoffman, M. J.: Basic complex analysis, 3rd ed. New York: W. H. Freeman 1999.
[14] Moulin, E., Grondel, G., Assaad, J.: Pseudo-3D modeling of a surface-bonded Lamb wave source (l). J. Acoust. Soc. Amer. **119**, 2575–2578 (2006).

Authors' addresses: S. von Ende and R. Lammering, Institute of Mechanics, Helmut-Schmidt-University / University of the Federal Armed Forces Hamburg, D-22043 Hamburg, Germany (E-mail: vonende@hsu-hh.de); I. Schäfer, Federal Armed Forces Underwater Acoustics and Marine Geophysics Research Institute, D-24148 Kiel, Germany